Biophysical Journal
Article

Biophysical Society

Emergence of Collagen Orientation Heterogeneity in Healing Infarcts and an Agent-Based Model

William J. Richardson[1,3] and Jeffrey W. Holmes[1,2,3,*]
[1]Department of Biomedical Engineering, [2]Department of Medicine, and [3]Robert M. Berne Cardiovascular Research Center, University of Virginia, Charlottesville, Virginia

ABSTRACT Spatial heterogeneity of matrix structure can be an important determinant of tissue function. Although bulk properties of collagen structure in healing myocardial infarcts have been characterized previously, regional heterogeneity in infarct structure has received minimal attention. Herein, we quantified regional variations of collagen and nuclear orientations over the initial weeks of healing after infarction in rats, and employed a computational model of infarct remodeling to test potential explanations for the heterogeneity we observed in vivo. Fiber and cell orientation maps were generated from infarct samples acquired previously at 1, 2, 3, and 6 weeks postinfarction in a rat ligation model. We analyzed heterogeneity by calculating the dot product of each fiber or cell orientation vector with every other fiber or cell orientation vector, and plotting that dot product versus distance between the fibers or cells. This analysis revealed prominent regional heterogeneity, with alignment of both fibers and cell nuclei in local pockets far exceeding the global average. Using an agent-based model of fibroblast-mediated collagen remodeling, we found that similar levels of heterogeneity can spontaneously emerge from initially isotropic matrix via locally reinforcing cell-matrix interactions. Specifically, cells that sensed fiber orientation at a distance or remodeled fibers at a distance by traction-mediated reorientation or aligned deposition gave rise to regionally heterogeneous structures. However, only the simulations in which cells deposited collagen fibers aligned with their own orientation reproduced experimentally measured patterns of heterogeneity across all time points. These predictions warrant experimental follow-up to test the role of such mechanisms in vivo and identify opportunities to control heterogeneity for therapeutic benefit.

INTRODUCTION

Fibrillar collagen is an abundant matrix component in many tissues and an important determinant of tissue mechanical properties. In particular, fiber orientation and alignment provide a structural basis for anisotropy, which is essential for the function of many load-bearing tissues, including tendons, ligaments, heart valves, and blood vessels. In some of these tissues, matrix structure and the resulting mechanical properties vary significantly across local subregions, and the effects of such heterogeneity are potentially important for tissue function or failure. For example, Vallabhaneni et al. (1) observed high variation in tensile moduli and strengths of human abdominal aortic aneurysm samples taken from different regions within the same aneurysms. They also found regional variation in matrix metalloproteinase 2 and 9 activities, consistent with observations by Hurks et al. (2), who found circumferential variation in abdominal aortic aneurysm structural composition (collagen, smooth muscle cells, inflammatory cells, and microvessels).

Collagen fiber structure is also an important determinant of the mechanics of scar tissue that forms after injury. We and others have quantified the collagen structure of healing myocardial infarcts and found that both collagen content and collagen fiber orientation vary widely across different experimental models (see a recent review by Richardson et al. (3)). Our group proposed that differences in the average degree of structural anisotropy in healing infarcts arise from differences in regional mechanics during scar formation (4). During the course of these studies, we noticed that collagen orientation in many of the scars we examined appeared to vary significantly from region to region. However, to our knowledge, no studies have quantified this spatial heterogeneity within healing infarcts or attempted to identify the mechanisms by which such heterogeneity arises. Understanding and controlling this heterogeneity could be therapeutically important because highly aligned strongly anisotropic scars yield better predicted pump function in computational models (5). Furthermore, it is possible that myocytes produced through

Submitted November 10, 2015, and accepted for publication April 7, 2016.
*Correspondence: holmes@virginia.edu
Editor: David Odde.
http://dx.doi.org/10.1016/j.bpj.2016.04.014

emerging regenerative approaches may align locally with the preexisting scar collagen, and heterogeneity in myocyte alignment would likely decrease contractile efficiency and increase the potential for arrhythmia. Accordingly, in this study we first quantified regional heterogeneity in healing myocardial infarcts in rats studied at four time points during the course of scar formation, and then utilized an agent-based model of scar formation to explore potential underlying mechanisms.

A variety of mechanisms could produce regional heterogeneity in scar collagen orientation, with the most intuitive being heterogeneity in chemical, mechanical, or preexisting structural cues that guide scar formation. As an alternative hypothesis, we propose that regional heterogeneity might also spontaneously emerge in the absence of any orienting guidance cues via locally reinforcing cell-cell or cell-matrix interactions. Fibroblasts are known to remodel their surrounding collagen matrix by exerting contractile forces on the fibers via transmembrane adhesions (e.g., integrins) while also degrading and depositing new collagen. In engineered tissue analogs, these forces pull collagen fibers into alignment with the cell's orientation, and in some cases cells also appear to deposit new fibers parallel to the cell orientation (6–8). Thus, fibroblast orientation can drive collagen orientation through multiple mechanisms. Conversely, cells are known to sense local structural cues and align themselves parallel to local fibers in a process termed contact guidance (9). Thus, collagen orientation can also drive fibroblast orientation. It is possible that this bidirectional interaction (cells determine collagen orientation, which in turn influences cell orientation) can result in a self-reinforcing, positive-feedback loop wherein local pockets of fiber alignment emerge from an initially homogeneous, randomly oriented mixture of fibers. This is especially plausible given the reports that cells can both sense and remodel collagen matrix properties over distances many times their own size (10–12). Accordingly, to test the hypothesis that heterogeneity in collagen fiber orientation in healing infarct scar can emerge spontaneously from cell-matrix interactions, we employed an agent-based model of infarct scar formation that was previously shown to predict average collagen fiber structure well across multiple experimental models (13).

MATERIALS AND METHODS

Infarct collagen and cell orientations

We previously acquired myocardial infarct samples at 1, 2, 3, and 6 weeks after permanent ligation of the left anterior descending coronary artery in rats (14). At the time of sacrifice, we arrested, excised, and sectioned hearts parallel to the epicardial plane and stained sections with either standard picrosirius red (PSR) or hematoxylin and eosin. For each of the four time points, we imaged sections from the midwall of four to five infarcts under 20× magnification with automated image stitching (Aperio ScanScope). We then generated collagen orientation maps from the PSR-stained images using a previously published image-processing method (15) (MatFiber, code freely available at http://bme.virginia.edu/holmes) implemented in MATLAB (The MathWorks, Natick, MA) that was previously used by our group to quantify collagen alignment in healing infarcts (4,14,16). This code segmented each PSR-stained image into a grid of 12 μm × 12 μm subregions, calculated intensity gradients within each subregion, and output a single angle for each subregion that was perpendicular to the maximum intensity gradient within that subregion (Fig. 1, *A* and *B*). Based on prior studies showing that nuclear orientation correlates closely with cell orientation (17), we quantified the orientation of elongated nuclei in infarct samples. We generated nuclear orientation maps from the hematoxylin and eosin-stained images using a custom image-processing code (implemented in MATLAB) that identified all nuclei in the image with an area of 2.5–50 μm^2 (to eliminate small debris and clumps of nuclei) and an elongation ratio (major axis/minor axis) of >1.5.

Alignment and heterogeneity metrics

To quantify global (average) alignment, we calculated the mean vector length (MVL), defined as follows:

$$\text{Global Alignment} = \text{MVL} = \sqrt{\left(\frac{\sum \cos(2\alpha_i)}{n}\right)^2 + \left(\frac{\sum \sin(2\alpha_i)}{n}\right)^2}, \quad (1)$$

where α_i is the set of orientation angles and n is the number of angles in the set (18). The angles are scaled by 2× to account for a bidirectional distribution (i.e., the angle range is −90:90 rather than −180:180).

To assess the regional heterogeneity of collagen and nuclear orientations, we first calculated the dot product of each orientation vector with every other orientation vector and plotted those dot products versus the distance between each vector pair. This resulted in a continuous distribution of alignment values across the range of distances. For averaging and plotting purposes, we binned the alignment values by incremental distance (0–20 μm, 20–40 μm, etc.), averaged the data within each bin in each infarct sample, and then averaged these per-bin values across the four to five samples to generate average alignment versus distance plots for each group (Fig. 1, *B* and *F*). For comparison, we rearranged the set of orientation measurements in each infarct by assigning each orientation vector a new, random location (Fig. 1 *C*), eliminating the correlation between alignment and distance (Fig. 1 *F*). We extracted the area between the original and rearranged alignment-versus-distance curves as a single measure that characterizes the degree to which local alignment exceeds global alignment (alignment area under the curve (AUC)).

Statistics

To statistically test for the presence of heterogeneity, we conducted a paired Student's *t*-test of fiber and cell AUC values against a hypothetical mean of zero (since a homogeneous material would yield AUC = 0). Statistical significance was set to 0.05 after Bonferroni corrections for multiple comparisons. To test for differences in AUC between cells versus fibers and for differences across time points, we conducted a two-way ANOVA using SPSS Statistics 23 (IBM). We also conducted this test for differences in MVL between groups.

Synthetic collagen fiber populations

For image processing, we segmented the collagen fiber network into 12 μm × 12 μm subregions before calculating an orientation vector for

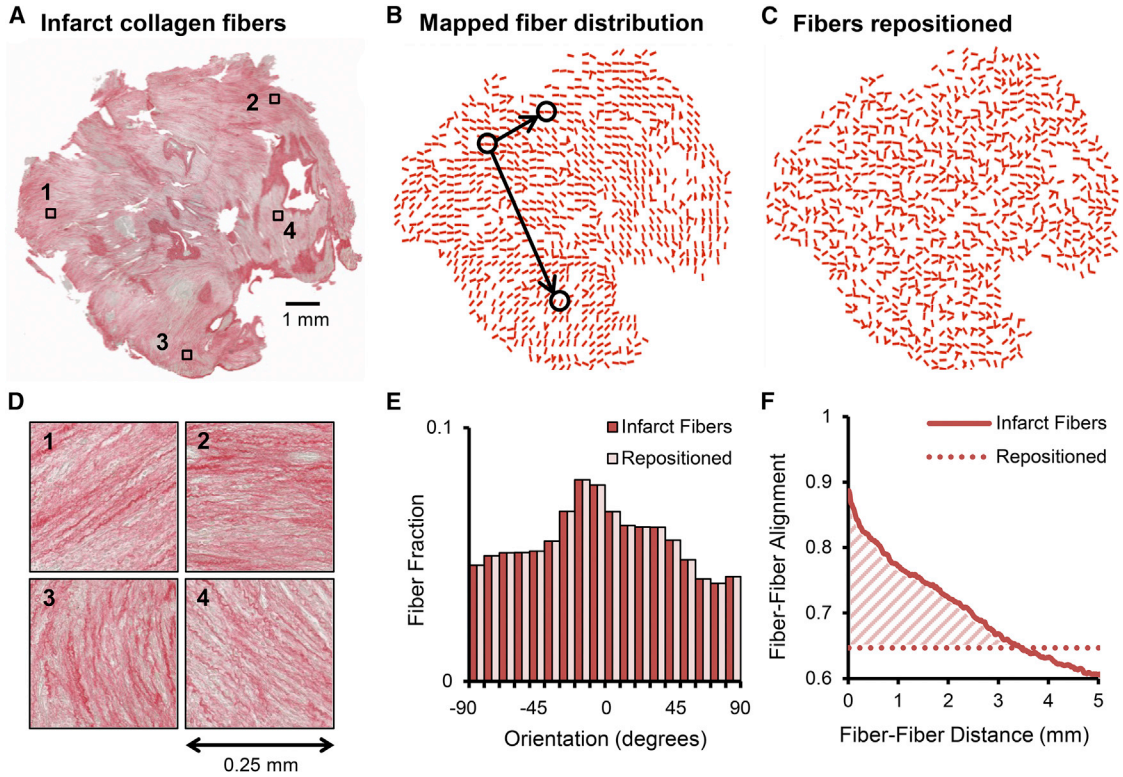

FIGURE 1 Quantification of regional heterogeneity in collagen fiber orientations. (*A*) Midwall sections from rat infarct scars were stained with PSR and imaged using an automated scanning system. (*D*) Local subregions displayed high alignment, but their average orientation varied across a given section. (*B*) To quantify regional heterogeneity, scanned images were processed to determine average orientation vectors in 12 μm $\times$ 12 μm regions. (*C* and *E*) For comparison, orientation vectors were randomly assigned new *x*-*y* positions, producing a population with the same average distribution but no local clustering. (*F*) Heterogeneity was analyzed by plotting the average alignment (dot product) between pairs of fibers versus the distance between them for both the experimental and repositioned orientation distributions. In the infarcts, nearby fibers were likely to be similarly aligned, whereas distant fibers were not. The shaded area represents the area between the original and repositioned alignment-versus-distance curves, providing a measure of the degree to which local alignment exceeds global alignment. To see this figure in color, go online.

each of those elements. In all subsequent heterogeneity analyses, we treated each vector as a distinct entity, even if two neighboring subregions were dominated by two neighboring portions of the same fiber or group of fibers. To analyze the impact of this choice on our heterogeneity analyses, we computationally generated two synthetic collagen fiber populations by randomly positioning either short fibers (15 μm) or long fibers (150 μm) with orientations drawn from the average distribution across our experimental samples. All fibers were straight with a width of 2 μm, consistent with typical fibers in our samples. We then converted both fiber populations into binary images and processed them in an identical fashion to infarct sections as described above. To account for stochasticity, we repeated this analysis with two additional replicate (but nonidentical) synthetic populations.

Agent-based infarct model

For computational modeling, we employed a previously published agent-based model of fibroblast-mediated collagen remodeling during infarct healing (13,19). Briefly, this model simulates cardiac fibroblasts as agents that follow rules to determine orientation, migration, collagen deposition, collagen degradation, and collagen reorientation, all according to local chemical, structural, and/or mechanical signals. The simulation space spans 8 mm $\times$ 8 mm centered around a 5-mm-diameter circular infarct. The space is discretized into 2.5 μm $\times$ 2.5 μm elements, with the collagen structure for each element saved as a distribution of fiber orientations in 5° bins from −90° to 90°. Cells are modeled as discs of 5 μm radius and are free to proliferate and migrate throughout the simulated infarct. For each time step, every cell senses and responds to mechanical, structural, and chemical cues. The mechanical cues are the directions and magnitudes of principal strains, structural cues are the directions and magnitudes of local collagen alignment, and chemical cues are the directions and magnitudes of the local gradient of a generic chemokine signal that simulates inflammatory mediators produced during healing.

We determined cell orientation in response to local cues by constructing vectors representing the strength and orientation of the local principal stretch, average fiber orientation, and chemokine gradient, averaging those vectors to obtain a mean orientation cue, and then constructing a probability distribution centered on the direction of the resultant vector and allowing the cell to randomly select a direction from that distribution. After reorientation and if space was available, cells migrated in the cell orientation direction with a speed dependent on the local chemokine magnitude. To simulate reorientation of collagen fibers by cell contractile forces, fiber distributions within a specified range of each cell were pulled toward that cell's orientation at a rate proportional to the angular distance between the collagen fiber orientation and cell orientation (Eq. 2). The collagen deposition rate depended on the local chemokine concentration, whereas degradation was a function of a global degradation rate and local collagen concentration (Eq. 3). We simulated cases in which cells could deposit collagen aligned with their orientation (aligned deposition), as well as cases

in which cells deposited randomly oriented collagen (random deposition).

$$\frac{d\theta_{Col}}{dt} = \begin{cases} k_{rotation}\|\sin(\theta_{cell} - \theta_{Col})\|, \ (\theta_{cell} - \theta_{Col}) \ in \ quadrants \ I, \ III \\ -k_{rotation}\|\sin(\theta_{cell} - \theta_{Col})\|, \ (\theta_{cell} - \theta_{Col}) in \ quadrants \ II, \ IV \end{cases} \quad (2)$$

$$\frac{\mathrm{d}[Col]}{\mathrm{d}t} = k_{deposition} - k_{degradation}[Col]. \quad (3)$$

The bulk of the model parameters were restrained to literature-reported values as described previously (13,19). One important difference compared with our previous modeling studies is that herein we simulated the infarct geometry in its full dimensions rather than scaling the problem, to maintain a physiologically accurate cell/infarct size ratio. Accordingly, we refit k_{rotation}, $k_{\mathrm{deposition}}$, and $k_{\mathrm{degradation}}$ to match the collagen content and alignment values measured in healing rat infarcts across a range of loading conditions (4,14). The model was solved using MATLAB.

Heterogeneity simulations

Since the aim of this study was to test whether regional heterogeneity could spontaneously emerge from an initially homogeneous environment in the absence of global alignment cues, we seeded an isotropic matrix of randomly oriented collagen (area fraction of 3%, typical of normal myocardium) with randomly positioned and randomly oriented cells (120,000, reflecting measured densities at 3 weeks) and simulated 3 weeks of matrix remodeling under equibiaxial loading (5% stretch) with a uniform chemokine concentration. Under these conditions, cells oriented based only on the local fiber orientation. More precisely, each cell picked an orientation from a wrapped normal distribution centered around the mean angle of the distribution of fiber orientations that the cell could sense. At baseline, the alignment of this cell orientation probability distribution was set equal to the MVL of the sensed fibers, but we explored the effect of varying the cell alignment strength by reducing the angular standard deviation of the cell orientation probability distribution, thereby making cells more likely to align with nearby collagen.

We considered three cell-matrix interactions that could give rise to regional heterogeneity in this simulation environment: 1) cells sensing and aligning with collagen (contact guidance), 2) cells depositing collagen aligned with their own orientation (aligned deposition), and 3) cells reorienting collagen into alignment with their own direction (reorientation) (Fig. S1 in the Supporting Material). To simplify comparisons between simulations, we allowed cells to remodel collagen via either reorientation or aligned deposition, but not both. To test the capability of these mechanisms to generate heterogeneity, we varied the rates and ranges over which these interactions occurred, predicted matrix remodeling for 3 weeks, and analyzed the predicted matrix structures for regional heterogeneity using the metrics described above.

For contact guidance simulations, each cell oriented itself based on the distribution of fiber orientations within a set distance from the cell. We varied this sensing range from 1 cell radius (i.e., cells sensed fibers only directly beneath them) to 50 cell radii. In addition to varying the sensing radius, we also varied the rates at which cells remodeled their matrix (i.e., the reorientation rate or turnover rate, depending on which remodeling mechanism was being simulated) from 1/4× to 4× the values that best reproduced global collagen alignment in our previous modeling studies. For remodeling simulations, cells oriented according to fibers within 1 cell radius, but remodeled fibers at a distance (via reorientation or aligned deposition). As with the contact guidance simulations, we varied the remodeling range from 1 cell radius to 50 cell radii, and the remodeling rates were varied from 1/4× to 4× experimental fits. In every case, four replicate simulations were run and averaged; these replicates yielded AUC values with a standard deviation < 5% of the mean, and alignment-versus-distance curves with a standard deviation also < 5% of the mean curve.

RESULTS

Infarct collagen and cell orientations are regionally heterogeneous

The average global levels of both collagen fiber and cell alignments were low across all healing time points assessed (Fig. 2, *A–C*). However, local subregions displayed strong alignment in directions that varied from subregion to subregion (Fig. 1, *A* and *D*). We assessed the observed heterogeneity quantitatively for fibers and cells by plotting the degree of coalignment (dot product) between pairs of fiber/cell alignment vectors versus the distance between those vectors (Fig. 2, *D* and *E*). From these plots, it is clear that fibers/cells near each other are more highly aligned than fibers/cells far away from each other. The AUC of the alignment-versus-distance curves was also quantified and averaged across rat infarct samples (Fig. 2 *F*, AUC significantly different from zero for all groups and time points, $p < 0.03$). This metric showed that the fibers and cells not only displayed similar levels of average global alignment (Fig. 2 *C*, ANOVA $p = 0.94$) but also showed similar levels of heterogeneity as assessed by the alignment AUC (Fig. 2 *F*, ANOVA $p = 0.14$). As discussed below, the features of the experimentally observed heterogeneity proved useful for differentiating potential underlying mechanisms in our model studies.

To assess potential artifacts introduced by segmenting the collagen network into 12 μm × 12 μm subregions for automated analysis of collagen fiber orientation, we performed identical image processing and heterogeneity analyses on two computationally generated fiber networks that matched the collagen density and global alignment averaged across our 1- to 6-week experimental samples, but contained randomly positioned short (15 μm) or long (150 μm) simulated collagen fibers (Fig. 3, *A* and *B*). This analysis revealed that because long fibers extend across neighboring regions, they do produce a local peak in our fiber-fiber alignment metric (Fig. 3 *C*), but the magnitude of that peak is far less than that observed in experimental infarct collagen networks and the effect fades far more rapidly with distance, disappearing completely in ~100 μm (less than one fiber length, Fig. 3 *C*), compared with 2–3 mm in our experimental measurements (Fig. 2 *D*).

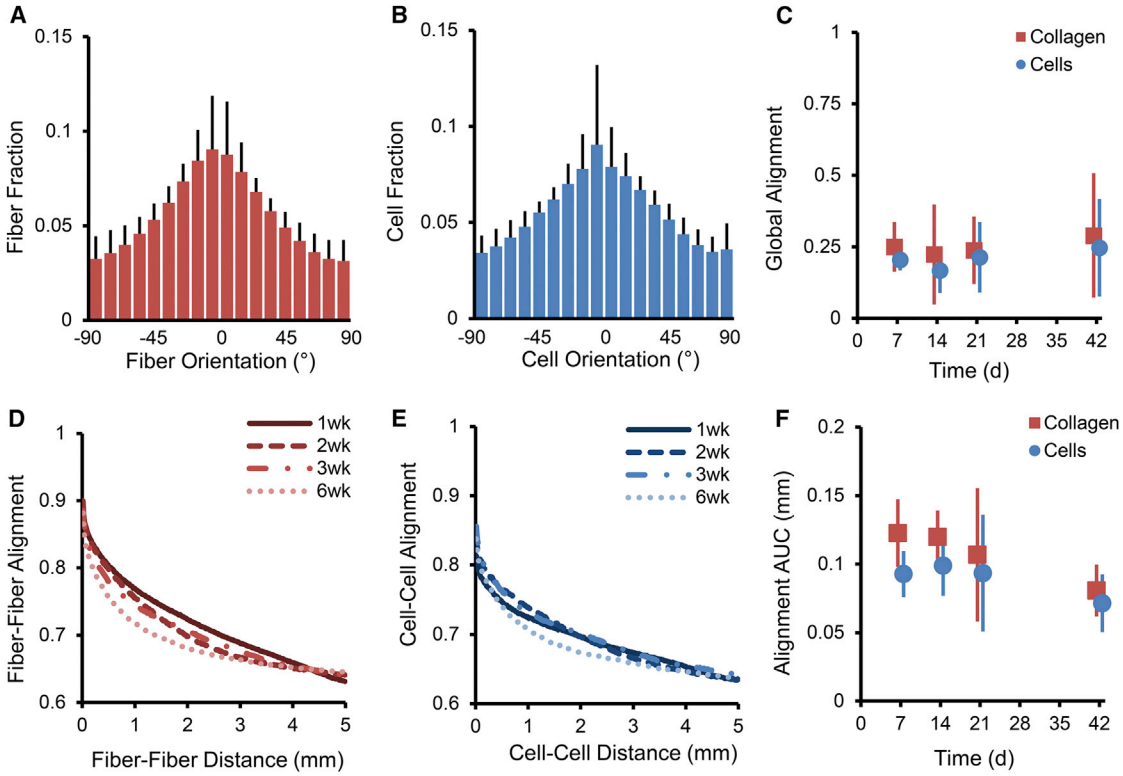

FIGURE 2 Collagen and cell orientations are regionally heterogeneous in healing rat infarcts. (*A–C*) Histograms of collagen fiber and cell orientations indicated low average alignment (*A* and *B*), which was quantified using a circular alignment measure, MVL (*C*). (*D* and *E*) Plotting the degree of coalignment (dot product) between pairs of alignment vectors versus the distance between those pairs clearly showed that fibers and cells close to each other were more highly aligned than fibers/cells far from each other. (*F*) From the alignment-versus-distance curves, we derived the alignment AUC metric, which showed that fibers and cells had similar levels of heterogeneity. To see this figure in color, go online.

Heterogeneity emerges in a model based on long-range cell-matrix interactions

To test the ability of cell-matrix interactions to spontaneously give rise to regional heterogeneity in collagen/cell orientations, we employed an agent-based model of a fibroblast population that sensed, deposited, degraded, and reoriented local matrix. The matrix was initially homogeneous and isotropic, with randomly oriented collagen fibers and randomly positioned, randomly oriented fibroblasts. Over 3 weeks of remodeling in the presence of isotropic, homogeneous mechanical and chemical cues, a clear regional

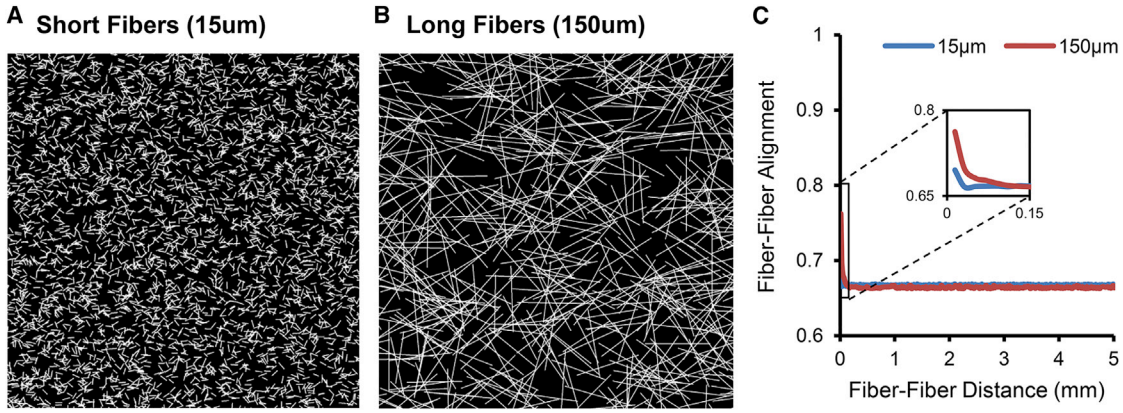

FIGURE 3 Collagen fiber length has a minor effect on heterogeneity analysis. (*A* and *B*) We generated synthetic fiber networks that matched the collagen density and global alignment averages of our 1- to 6-week rat ligation infarct samples by randomly positioning short (*A*, 15 μm) or long (*B*, 150 μm) fibers. (*C*) Long fibers produced an apparent coalignment of adjacent regions in our automated analysis, but the magnitude and spatial extent of this effect were very small compared with the measured curves from experimental infarct sections (cf. Fig. 2 *D*). To see this figure in color, go online.

heterogeneity in fiber orientations spontaneously emerged under some of the conditions tested, but both the presence and the degree of heterogeneity depended upon the rate, spatial range, and type of cell-matrix interactions as described below (Figs. 4, 5, 6, S2, and S3).

Regardless of the type of cell-matrix interaction, the most critical parameter governing fiber and cell heterogeneity was the interaction range. As cells have previously been shown to interact with their substrate over long distances (10–12), we tested the effect of cells either sensing or remodeling fibers over variable ranges, from 1 cell radius to 50 cell radii (Fig. 4). Although short-range interactions over 1 cell radius did not produce any substantial heterogeneity, long-range aligned deposition (Fig. 4 *A*), long-range sensing with local aligned deposition (Fig. 4 *B*), long-range reorientation (Fig. 4 *C*), and long-range sensing with local reorientation (Fig. 4 *D*) were all able to generate both fiber and cell heterogeneity by 3 weeks to a degree that was proportional to the range of interaction. In agreement with the experimental findings, in most simulations, fibers and cells exhibited comparable levels of heterogeneity as evidenced by alignment-versus-distance plots (Fig. 4) and AUC measurements (Figs. S2 and S3). Notably, the emergent heterogeneity extended over distances that were much larger than the cell-fiber interaction distance, e.g., cells that remodeled across 50 times their radius produced pockets of alignment extending ~300 times their radius.

Although multiple different simulations produced heterogeneity, the time course over which that heterogeneity emerged varied (Fig. 5). Long-range aligned deposition and long-range sensing with local aligned deposition produced a sudden emergence of heterogeneity by week 1, which remained essentially the same over the subsequent weeks of healing (Fig. 5, *A* and *C*). Importantly, this agrees with the experimental curves, which show that heterogeneity was established by week 1 and remained unchanged across 1–6 weeks (Fig. 2, *D–F*). In contrast, long-range reorientation and long-range sensing with local reorientation produced gradually increasing heterogeneity as evidenced by incremental shifts of the alignment-versus-distance curves (Fig. 5, *B* and *D*) and gradually increasing AUC values (Figs. S2 and S3).

We also explored the effect of the remodeling rate on the degree of heterogeneity (Figs. S2 and S3). Changing collagen turnover rates from 1/4 to 4 times the baseline rate had a minimal effect on fiber and cell heterogeneities for either long-range aligned deposition or long-range sensing with aligned deposition. However, changing the reorientation rates from 1/4 to 4 times the baseline rate had significant effects on fiber and cell heterogeneities for

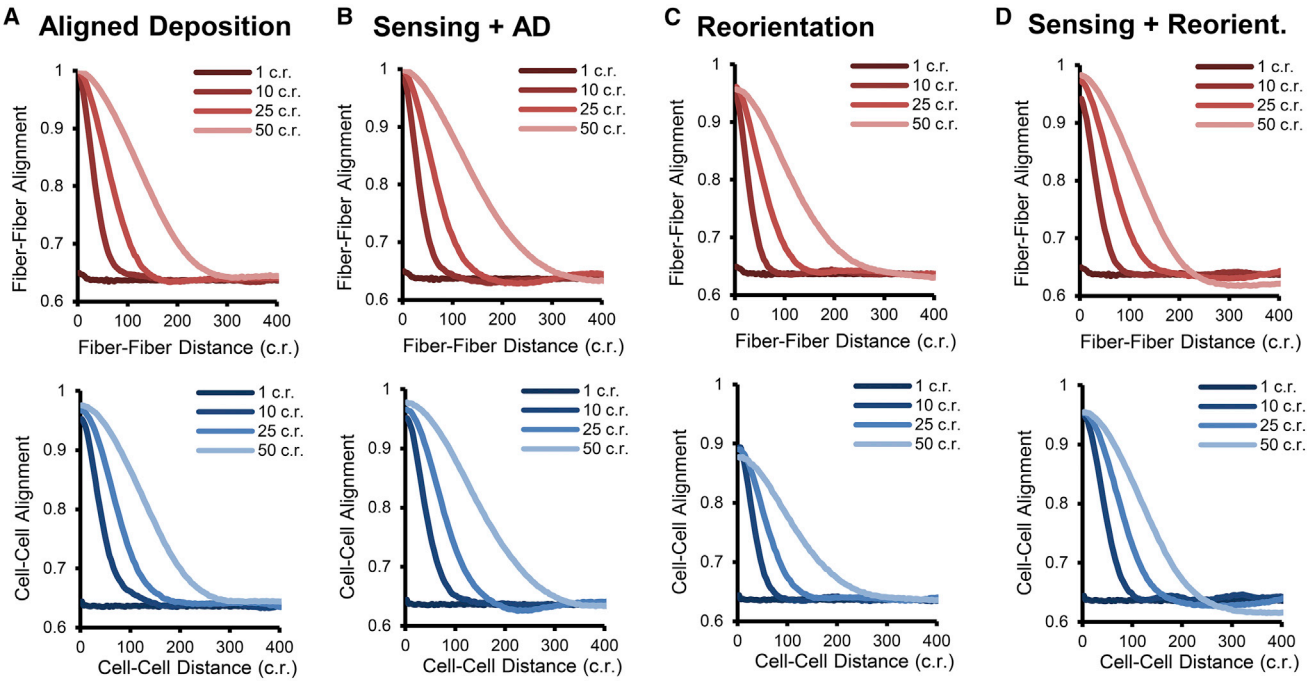

FIGURE 4 Spontaneous emergence of regional heterogeneity in model simulations. Even with homogeneous and isotropic mechanical and chemical cues, regional heterogeneity emerged spontaneously via cell-matrix interactions in the ABM. The emergence and degree of heterogeneity depended upon the interaction mechanism, interaction range, and remodeling rates, but the strongest determinant of heterogeneity was range. (*A–D*) Across all types of interaction mechanisms, collagen and cell heterogeneity after 3 weeks of remodeling were proportional to the distance of long-range aligned deposition (*A*), long-range reorientation (*C*), or long-range sensing (*B* and *D*). Short-range interactions (i.e., range = 1 cell radius) did not generate any substantial heterogeneity. Results from the full range of parameters tested can be found in Figs. S2 and S3. For the simulations shown, remodeling rates were set to equal baseline values and the cell alignment strength = 2/5 standard deviation. To see this figure in color, go online.

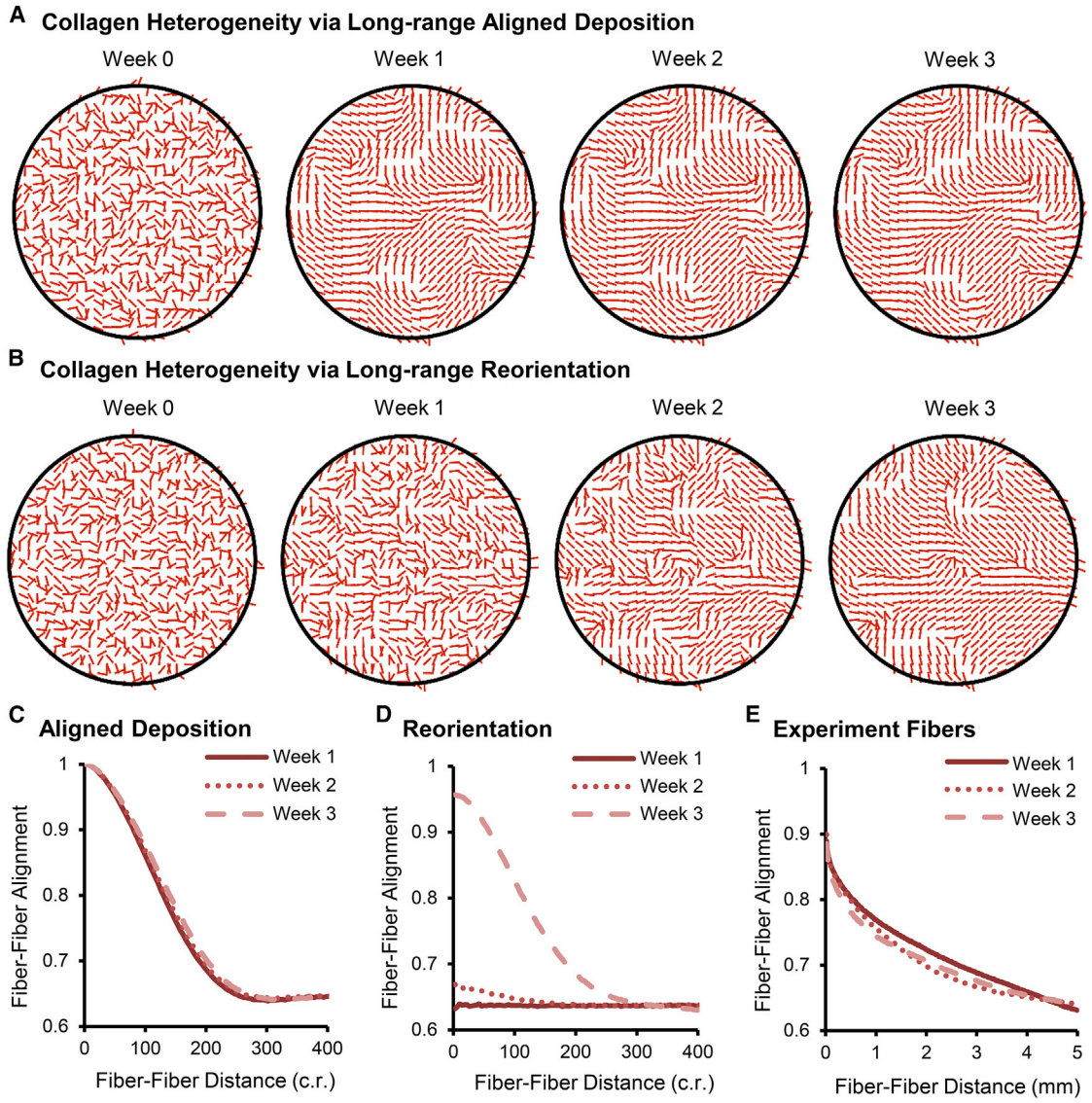

FIGURE 5 Time courses of regional heterogeneity in model simulations. Initial collagen structures were randomly oriented with randomly oriented, randomly positioned cells. (*A* and *B*) Over 3 weeks of simulated remodeling, distinctly visible regional heterogeneity in collagen orientations spontaneously emerged in both long-range aligned deposition (*A*) and long-range reorientation (*B*) simulations. (*C* and *D*) However, the time courses differed in these two cases: aligned deposition produced a sudden and early appearance of heterogeneity that remained stable (*C*), whereas reorientation produced a gradual increase in heterogeneity as evident in slowly rising fiber-fiber alignment-versus-distance curves (*D*). The same trends were true for long-range sensing with aligned deposition (sudden appearance; Fig. S3) versus long-range sensing with reorientation (gradual appearance; Fig. S3). For comparison, heterogeneity in the experimental measurements appeared by week 1 and remained stable through the rest of the healing time course (*E*). The parameters for these simulations were baseline remodeling rates, interaction range = 50 cell radii, and cell alignment strength = 2/5 standard deviation. To see this figure in color, go online.

both long-range reorientation and long-range sensing with reorientation. In fact, decreasing the reorientation rate to just 1/2 its baseline value completely eliminated heterogeneity in the long-range reorientation simulation. As detailed in the Materials and Methods section, one additional parameter that we varied in these simulations was the width of the cell orientation probability distribution, which controls how strongly a cell aligns with the fibers that it senses. The degree of predicted heterogeneity depended on this cell alignment strength across all interaction mechanisms (Figs. S2 and S3).

It is possible that in vivo, cells are not uniformly distributed, as we simulated in this study. To test whether an extreme case of cell clustering might produce fiber heterogeneity, we performed simulations that began with 75% of cells clustered into 13 evenly spaced groups and 25% of cells randomly scattered (Fig. 6 *A*). After 21 days of remodeling via either reorientation or aligned deposition, both cell and fiber heterogeneity emerged even when cells only sensed and remodeled locally (range = 1 cell radius, Fig. 6, *B* and *C*). Not surprisingly, the spatial orientation pattern followed the cell cluster positions, and the

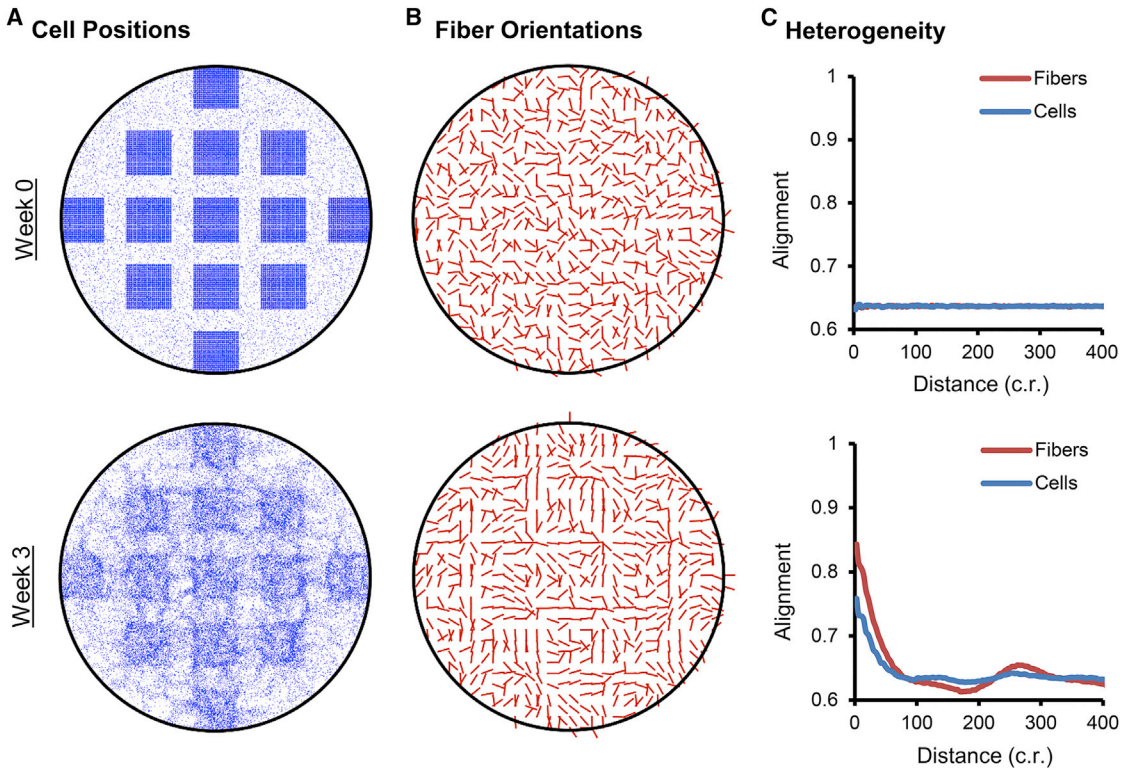

FIGURE 6 Effect of cell clustering on regional heterogeneity. (*A*) Initial collagen and cells were randomly oriented, but 75% of the cells were positioned in 13 evenly spaced clusters. Structure was allowed to remodel for 3 weeks via either aligned deposition or reorientation mechanisms, but cell sensing and cell remodeling were short-ranged (i.e., 1 cell radius). (*B* and *C*) After 3 weeks, both fiber and cell regional heterogeneity emerged even without long-range interactions. The spatial pattern of heterogeneity seemed to correspond with initial cell cluster positions, and alignment-versus-distance plots exhibited interesting oscillatory behavior, also seemingly corresponding to cluster distances (*C*). The parameters for the simulation shown were aligned deposition with baseline turnover rate, turnover range = 1 cell radius, sensing range = 1 cell radius, and cell alignment strength = 2/5 standard deviation. To see this figure in color, go online.

alignment-distance plot exhibited an oscillatory pattern that also corresponded to the cluster distances. However, the degree of heterogeneity was small when compared with the experimentally observed levels or the levels generated in simulations that included long-range interactions.

DISCUSSION

The collagen fiber structure of healing infarcts is a key determinant of their mechanical properties, which in turn influence left ventricular function as well as the risk of postinfarction complications such as infarct rupture and the development of heart failure (20). We (4,14,21) and others (22) have reported a range of collagen fiber structures in healing infarcts in different animal models, and have shown that manipulating anisotropy in healing infarcts can improve left ventricular pump function (5,23). These prior studies focused on collagen content and alignment averaged over many microscopic fields; broadly, they show collagen fibers oriented in planes parallel to the epicardial surface, with a degree of overall alignment that depends strongly on the mechanical environment during scar formation (4). However, over the course of our studies, we also observed a striking structural heterogeneity: local pockets of highly aligned collagen fibers with orientations that varied substantially across different locations within the same histologic section. To our knowledge, this study is the first attempt to quantify that heterogeneity and use computational modeling to explore hypotheses about its origin.

Structural heterogeneity in healing rat infarcts

We constructed metrics to quantify heterogeneity by assessing how strongly nearby-versus-distant collagen fibers were aligned with one another. We found that in healing rat myocardial infarcts, nearby fibers were much more strongly aligned with one another than fibers separated by larger distances, despite the fact that average collagen fiber alignment was low across the entire sample. This pattern of structural heterogeneity appeared by 1 week postinfarction and then changed little over the next 5 weeks, despite progressive accumulation of collagen. The results of a similar analysis applied to elongated cell nuclei in the same images suggested that there is comparable heterogeneity in cell alignment and collagen alignment. The reported cell alignment and heterogeneity values shown here included all elongated

nuclei with an aspect ratio of ≥ 1.5. Raising/lowering this threshold slightly increased/decreased the resulting cell alignment and heterogeneity metrics without changing any of the qualitative findings we reported. Plausible mechanisms for the genesis of regional heterogeneity must explain not only how such patterns can arise but also why they emerge so early during healing, and how both collagen fibers and cells end up similarly aligned.

There is some evidence that regional heterogeneity can alter failure properties (24); however, we are unable to draw conclusions regarding possible contributions of the heterogeneity we observed to the likelihood of infarct rupture. In vivo, most infarct ruptures occur in the first few days after infarction (25–27), whereas our earliest time point was 1 week. However, structural heterogeneity in healing myocardial infarcts certainly has at least one other important implication in this era of emerging cardiac regenerative therapies: cardiomyocytes have been shown to align with preexisting matrix (28), and heterogeneity in regenerated myocyte alignment could impair both electrical and mechanical functions of the myocardium.

Mechanisms for generating heterogeneity: long-range sensing

Cells are able to sense substrate stiffness up to at least 150 μm (12). It is unclear whether they can also sense fiber orientations at comparable distances, but it seems plausible that if those fiber orientations confer mechanical anisotropy, then cells might be able to sense that anisotropy over similar distances. Across the parameter ranges we simulated, long-range sensing of fiber orientations (contact guidance) was able to produce substantial heterogeneity in both collagen and cell orientations in proportion to the sensing distance. As each cell sensed and aligned with fibers over large distances, groups of cells would coalign with each other and then deposit or reorient fibers into their shared direction, thereby influencing the orientation preference for other nearby cells. Importantly, long-range sensing was able to produce comparable degrees of collagen and cell heterogeneity, which agrees with the experimental infarct data. However, other features of the emergent heterogeneity depended upon how cells influenced fiber orientation, i.e., via aligned deposition or reorientation, as discussed below (Figs. 5 and S2). We should also note that the ability of long-range sensing to generate heterogeneity depended upon how strongly cells aligned with the mean fiber orientation within their sensing range, and that heterogeneity emerged from long-range sensing only when cells aligned more strongly than the fibers they sensed. The biological implications of this finding are not immediately clear, because cells in the model choose orientations randomly from a probability distribution based only on current environmental cues, whereas the behavior of actual cells in vivo likely includes some history dependence.

Mechanisms for generating heterogeneity: aligned deposition of collagen fibers

As cells move and deposit collagen, in some situations they appear to deposit fibers parallel to their own orientation (6–8). Accordingly, we tested the effects of allowing cells to deposit collagen aligned with their orientation over regions of variable size. In these simulations, cells chose their initial orientations randomly, since no global orientation cues were provided. Then, once a cell began to deposit collagen aligned with its orientation, nearby cells began to align with that collagen, creating local reinforcement of the initial cell orientations. Like long-range sensing, long-range aligned deposition allowed cells to generate a degree of fiber and cell heterogeneity that depended upon the range of interaction, and again, fibers and cells showed comparable degrees of heterogeneity. We also found that this mechanism reproduced a key feature of the experimental infarct data: heterogeneity emerged within the first few days of simulated healing and was maintained at similar levels throughout the remaining time course. Thus, both local sensing with long-range aligned deposition (Fig. S3, *A* and *B*) and long-range sensing with local aligned deposition (Fig. S2, *A* and *B*) can give rise to heterogeneous structures that match the critical features we observed in healing rat infarcts. The idea of cells depositing collagen fibers at a distance is obviously a somewhat artificial model construct. However, it may be possible that the local orientation of collagen monomers or fibrils produced by a cell could help determine the orientation of larger collagen fibers that form by aggregation of those smaller subunits, influencing collagen orientation over distances of hundreds of microns. Thus, although we did not think that enough is known about the control of orientation during fibrillogenesis to explicitly include these effects in our model, our results suggest that the role of fibrillogenesis in controlling collagen fiber alignment and heterogeneity warrants further study and modeling (e.g., (29–32)).

Mechanisms for generating heterogeneity: reorientation of collagen fibers

By exerting local traction via integrin-matrix connections, cells can deform and reorient fibrillar matrices over hundreds of microns (10,11). Accordingly, we tested the ability of such long-range fiber reorientation to give rise to fiber heterogeneity in our computational model. Like long-range sensing and long-range aligned deposition, long-range reorientation was able to generate both fiber and cell heterogeneity to a degree that depended upon the distance over which cells reoriented fibers. However, local sensing with long-range reorientation (Fig. S3, *C* and *D*) and long-range sensing with local reorientation (Fig. S2, *C* and *D*) both failed to reproduce the time course of heterogeneity that we observed in the rat infarcts. Specifically, whereas experimentally measured heterogeneity emerged quickly and

remained consistent after 1 week, simulated heterogeneity from reorientation emerged gradually over the healing time course. In addition, the degree of heterogeneity in all reorientation simulations was highly dependent upon the rate at which the cells could reorient fibers: decreasing the reorientation rate by half completely eliminated the emergence of heterogeneity. We should note that reorientation of collagen fibers was represented phenomenologically in our model by modification of local orientation distributions. This approach did not simulate the actual deformation of individual fibers or the surrounding matrix by cell tractions, or other important mechanical phenomena such as entanglement of the fibers. Thus, it is possible that a more detailed model of traction-mediated remodeling could produce different results, for example, with respect to the temporal development of heterogeneity. However, regardless of the details of the model implementation, it is unclear to us whether fibroblasts could physically generate the degree and spatial extent of physical reorientation modeled here in a dense, solid tissue experiencing cyclic stresses on the order of tens of kilopascals with every heartbeat.

Mechanisms for generating heterogeneity: preexisting structure

One obvious alternative explanation for scar heterogeneity is that fibroblast and/or collagen fiber orientation is guided by some preexisting heterogeneous structural cue. However, previous histologic studies of other structures that might survive the initial infarct and serve as structural templates did not reveal any plausible candidates. Myocytes (and the extracellular matrix that surrounds them) tend to be highly and consistently aligned across large distances in myocardium sectioned parallel to the epicardial surface (33,34). Furthermore, in our own samples, we could not consistently associate local pockets of aligned collagen fibers with any adjacent structures such as blood vessels. We did explore the effects of nonuniform cell densities on heterogeneity and found that indeed, extreme cell clustering could give rise to some heterogeneity in fiber and cell orientations. However, the degree of this heterogeneity was substantially less than that observed experimentally or achieved in long-range interaction simulations.

Other models in the literature

Investigators have developed a number of computational approaches to predict fibrous matrix remodeling in response to chemical, structural, and/or mechanical inputs using a variety of frameworks, including continuum, finite-element, and agent-based models. Some of these models have produced heterogeneous predicted fiber structures, although to our knowledge no prior study has explicitly sought to explain the genesis of experimentally measured heterogeneity. Baaijens and colleagues (35–40) solved structure-based constitutive relations in continuous or finite-element models of arterial wall and aortic valve, assuming a preferred fiber direction either parallel or in between local principal strain or stress directions. Their models correctly predicted the hammock-like heterogeneous distribution of matrix orientation in heart valves and the helical arrangement of matrix fibers in arterial walls. In these simulations, the mean fiber orientation varied spatially due to the geometry and boundary conditions of the simulated tissue. By contrast, in our models the mean fiber orientation was random due to the lack of a dominant orientation cue, whereas local alignment emerged spontaneously.

Checa et al. (41) used a hybrid approach combining finite-element and agent-based models to capture mechanical interactions between fiber networks and cells, simulated as contractile force dipoles. Cells oriented and migrated based on the resultant mechanical equilibrium after contracting against the fiber network, and showed a migration tendency toward stiffer neighboring elements. Fibers were assumed to reorient toward the direction of principal stress. These simulations resulted in distinct cell-clumping patterns and appeared to produce regionally heterogeneous fiber orientations, but this heterogeneity was not quantified or discussed. Reinhardt and Gooch (42) also used an agent-based model to simulate two contractile cells embedded within a network of fiber segments modeled as Hookean and torsional springs. These simulations predicted compaction and alignment of fibers between the cells, but heterogeneity was again not addressed. Hoffmann et al. (43) used an agent-based model to predict in vitro mesenchymal cell organization based on attractive and repulsive forces between elongated cells and underlying substrate during proliferation, migration, and crowding. Those interactions did lead to regional heterogeneity in cell orientations, as was evident in a plot of alignment versus distance. However, the length scale of heterogeneity was nearly 2 orders of magnitude shorter than our simulations ($<$10 cell radii versus hundreds of cell radii).

The published models most similar to ours are the hybrid continuum+agent-based models developed by Dallon et al. (44–46) and McDougall et al. (47) to simulate fibroblast-mediated wound repair, in which cells orient, migrate, and rearrange collagen according to local fiber structure and chemokine gradients. Their models also predicted heterogeneous structures: high fiber alignment within local regions on the order of 100μm (44), quantified by plotting fiber alignment versus window size (the distance over which fibers were grouped to calculate alignment, a method inspired by Rand and Wilson (48)). But in contrast to our study, their simulations began with some initial heterogeneity as a result of randomized fiber seeding, whereas the heterogeneity in our simulations spontaneously emerged from an initially homogeneous environment.

CONCLUSIONS

In summary, both fiber and cell orientations in healing rat infarcts were regionally heterogeneous and the degree of heterogeneity was stable across the healing time course of 1–6 weeks. Agent-based model simulations showed that such heterogeneity can spontaneously emerge from an initially homogeneous matrix as a result of cell-matrix interactions over large distances. Mechanisms by which individual cells remodeled collagen at a distance (via aligned deposition of new fibers or reorientation of existing fibers) or sensed at a distance generated fiber and cell heterogeneity. Further, local sensing with long-range aligned deposition and long-range sensing with local aligned deposition reproduced all features of the experimental data, including the time course of heterogeneity development. In vivo, the role of such spontaneous emergence versus spatially varying chemical or mechanical cues remains unclear, as do the specific biologic mechanisms (if any) by which cells might influence alignment of collagen fibers over relatively long distances. Still, our simulations suggest that by identifying and understanding such mechanisms, we may gain insight into how to therapeutically manipulate regional heterogeneity in healing scar tissue.

SUPPORTING MATERIAL

Three figures are available at http://www.biophysj.org/biophysj/supplemental/S0006-3495(16)30177-1.

AUTHOR CONTRIBUTIONS

W.J.R. and J.W.H. designed the experimental analysis and computational simulations, discussed the results, and wrote/edited the manuscript. W.J.R. performed the experimental analysis and computational simulations.

ACKNOWLEDGMENTS

The authors thank Kamal Chikalard for assisting with infarct section imaging.

This work was supported by the National Institutes of Health (2T32HL007284 to W.J.R. and R01 HL116449 to J.W.H.), the American Heart Association (14POST20460271 to W.J.R.), and the National Science Foundation (CMMI 1332530 to J.W.H.).

REFERENCES

1. Vallabhaneni, S. R., G. L. Gilling-Smith, …, P. L. Harris. 2004. Heterogeneity of tensile strength and matrix metalloproteinase activity in the wall of abdominal aortic aneurysms. *J. Endovasc. Ther.* 11:494–502.
2. Hurks, R., G. Pasterkamp, …, F. L. Moll. 2012. Circumferential heterogeneity in the abdominal aortic aneurysm wall composition suggests lateral sides to be more rupture prone. *J. Vasc. Surg.* 55:203–209.
3. Richardson, W. J., S. A. Clarke, …, J. W. Holmes. 2015. Physiological implications of myocardial scar structure. *Compr. Physiol.* 5:1877–1909.
4. Fomovsky, G. M., A. D. Rouillard, and J. W. Holmes. 2012. Regional mechanics determine collagen fiber structure in healing myocardial infarcts. *J. Mol. Cell. Cardiol.* 52:1083–1090.
5. Fomovsky, G. M., J. R. Macadangdang, …, J. W. Holmes. 2011. Model-based design of mechanical therapies for myocardial infarction. *J. Cardiovasc. Transl. Res.* 4:82–91.
6. Birk, D. E., and R. L. Trelstad. 1986. Extracellular compartments in tendon morphogenesis: collagen fibril, bundle, and macroaggregate formation. *J. Cell Biol.* 103:231–240.
7. Trelstad, R. L., and K. Hayashi. 1979. Tendon collagen fibrillogenesis: intracellular subassemblies and cell surface changes associated with fibril growth. *Dev. Biol.* 71:228–242.
8. Canty, E. G., Y. Lu, …, K. E. Kadler. 2004. Coalignment of plasma membrane channels and protrusions (fibripositors) specifies the parallelism of tendon. *J. Cell Biol.* 165:553–563.
9. Dunn, G. A., and J. P. Heath. 1976. A new hypothesis of contact guidance in tissue cells. *Exp. Cell Res.* 101:1–14.
10. Wang, H., A. S. Abhilash, …, V. B. Shenoy. 2014. Long-range force transmission in fibrous matrices enabled by tension-driven alignment of fibers. *Biophys. J.* 107:2592–2603.
11. Harris, A. K., D. Stopak, and P. Wild. 1981. Fibroblast traction as a mechanism for collagen morphogenesis. *Nature.* 290:249–251.
12. Rudnicki, M. S., H. A. Cirka, …, K. L. Billiar. 2013. Nonlinear strain stiffening is not sufficient to explain how far cells can feel on fibrous protein gels. *Biophys. J.* 105:11–20.
13. Rouillard, A. D., and J. W. Holmes. 2012. Mechanical regulation of fibroblast migration and collagen remodelling in healing myocardial infarcts. *J. Physiol.* 590:4585–4602.
14. Fomovsky, G. M., and J. W. Holmes. 2010. Evolution of scar structure, mechanics, and ventricular function after myocardial infarction in the rat. *Am. J. Physiol. Heart Circ. Physiol.* 298:H221–H228.
15. Karlon, W. J., J. W. Covell, …, J. H. Omens. 1998. Automated measurement of myofiber disarray in transgenic mice with ventricular expression of ras. *Anat. Rec.* 252:612–625.
16. Clarke, S. A., N. C. Goodman, …, J. W. Holmes. 2015. Effect of scar compaction on the therapeutic efficacy of anisotropic reinforcement following myocardial infarction in the dog. *J. Cardiovasc. Transl. Res.* 8:353–361.
17. McKee, C. T., V. K. Raghunathan, …, C. J. Murphy. 2011. Topographic modulation of the orientation and shape of cell nuclei and their influence on the measured elastic modulus of epithelial cells. *Biophys. J.* 101:2139–2146.
18. Zar, J. H. 2010. Biostatistical Analysis, 5th ed. Prentice Hall, Englewood Cliffs, NJ.
19. Rouillard, A. D., and J. W. Holmes. 2014. Coupled agent-based and finite-element models for predicting scar structure following myocardial infarction. *Prog. Biophys. Mol. Biol.* 115:235–243.
20. Holmes, J. W., T. K. Borg, and J. W. Covell. 2005. Structure and mechanics of healing myocardial infarcts. *Annu. Rev. Biomed. Eng.* 7:223–253.
21. Holmes, J. W., J. A. Nuñez, and J. W. Covell. 1997. Functional implications of myocardial scar structure. *Am. J. Physiol.* 272:H2123–H2130.
22. Whittaker, P., D. R. Boughner, and R. A. Kloner. 1989. Analysis of healing after myocardial infarction using polarized light microscopy. *Am. J. Pathol.* 134:879–893.
23. Fomovsky, G. M., S. A. Clark, …, J. W. Holmes. 2012. Anisotropic reinforcement of acute anteroapical infarcts improves pump function. *Circ Heart Fail.* 5:515–522.
24. Hadi, M. F., and V. H. Barocas. 2013. Microscale fiber network alignment affects macroscale failure behavior in simulated collagen tissue analogs. *J. Biomech. Eng.* 135:021026.
25. Gao, X.-M., D. A. White, …, X.-J. Du. 2012. Post-infarct cardiac rupture: recent insights on pathogenesis and therapeutic interventions. *Pharmacol. Ther.* 134:156–179.

26. Batts, K. P., D. M. Ackermann, and W. D. Edwards. 1990. Postinfarction rupture of the left ventricular free wall: clinicopathologic correlates in 100 consecutive autopsy cases. *Hum. Pathol.* 21:530–535.
27. Purcaro, A., C. Costantini, …, D. Astolfi. 1997. Diagnostic criteria and management of subacute ventricular free wall rupture complicating acute myocardial infarction. *Am. J. Cardiol.* 80:397–405.
28. Kai, D., M. P. Prabhakaran, …, S. Ramakrishna. 2011. Guided orientation of cardiomyocytes on electrospun aligned nanofibers for cardiac tissue engineering. *J. Biomed. Mater. Res. B Appl. Biomater.* 98:379–386.
29. Silver, D., and J. Miller. 1994. Visualizing collagen fibril growth. *J. Mol. Graph.* 12:139–145.
30. Parkinson, J., K. E. Kadler, and A. Brass. 1995. Simple physical model of collagen fibrillogenesis based on diffusion limited aggregation. *J. Mol. Biol.* 247:823–831.
31. Parkinson, J., K. E. Kadler, and A. Brass. 1994. Self-assembly of rodlike particles in two dimensions: a simple model for collagen fibrillogenesis. *Phys. Rev. E Stat. Phys. Plasmas Fluids Relat. Interdiscip. Topics.* 50:2963–2966.
32. Hulmes, D. J., T. J. Wess, …, P. Fratzl. 1995. Radial packing, order, and disorder in collagen fibrils. *Biophys. J.* 68:1661–1670.
33. Streeter, D. D., Jr., and W. T. Hanna. 1973. Engineering mechanics for successive states in canine left ventricular myocardium. II. Fiber angle and sarcomere length. *Circ. Res.* 33:656–664.
34. Nielsen, P. M., I. J. Le Grice, …, P. J. Hunter. 1991. Mathematical model of geometry and fibrous structure of the heart. *Am. J. Physiol.* 260:H1365–H1378.
35. Driessen, N. J., R. A. Boerboom, …, F. P. Baaijens. 2003. Computational analyses of mechanically induced collagen fiber remodeling in the aortic heart valve. *J. Biomech. Eng.* 125:549–557.
36. Driessen, N. J. B., C. V. C. Bouten, and F. P. T. Baaijens. 2005. Improved prediction of the collagen fiber architecture in the aortic heart valve. *J. Biomech. Eng.* 127:329–336.
37. Driessen, N. J. B., M. A. J. Cox, …, F. P. T. Baaijens. 2008. Remodelling of the angular collagen fiber distribution in cardiovascular tissues. *Biomech. Model. Mechanobiol.* 7:93–103.
38. Machyshyn, I. M., P. H. M. Bovendeerd, …, F. N. van de Vosse. 2010. A model for arterial adaptation combining microstructural collagen remodeling and 3D tissue growth. *Biomech. Model. Mechanobiol.* 9:671–687.
39. Driessen, N. J. B., W. Wilson, …, F. P. T. Baaijens. 2004. A computational model for collagen fibre remodelling in the arterial wall. *J. Theor. Biol.* 226:53–64.
40. Baaijens, F., C. Bouten, and N. Driessen. 2010. Modeling collagen remodeling. *J. Biomech.* 43:166–175.
41. Checa, S., M. K. Rausch, …, G. N. Duda. 2015. The emergence of extracellular matrix mechanics and cell traction forces as important regulators of cellular self-organization. *Biomech. Model. Mechanobiol.* 14:1–13.
42. Reinhardt, J. W., and K. J. Gooch. 2014. Agent-based modeling traction force mediated compaction of cell-populated collagen gels using physically realistic fibril mechanics. *J. Biomech. Eng.* 136:021024.
43. Hoffmann, M., J.-P. Kuska, …, J. Galle. 2011. Spatial organization of mesenchymal stem cells in vitro–results from a new individual cell-based model with podia. *PLoS One.* 6:e21960.
44. Dallon, J. C., J. A. Sherratt, and P. K. Maini. 1999. Mathematical modelling of extracellular matrix dynamics using discrete cells: fiber orientation and tissue regeneration. *J. Theor. Biol.* 199:449–471.
45. Dallon, J., J. Sherratt, …, M. Ferguson. 2000. Biological implications of a discrete mathematical model for collagen deposition and alignment in dermal wound repair. *IMA J. Math. Appl. Med. Biol.* 17:379–393.
46. McDougall, S., J. Dallon, …, P. Maini. 2006. Fibroblast migration and collagen deposition during dermal wound healing: mathematical modelling and clinical implications. *Philos. Trans. A Math Phys. Eng. Sci.* 364:1385–1405.
47. Dallon, J. C., J. A. Sherratt, and P. K. Maini. 2001. Modeling the effects of transforming growth factor-beta on extracellular matrix alignment in dermal wound repair. *Wound Repair Regen.* 9:278–286.
48. Rand, D. A., and H. B. Wilson. 1995. Using spatio-temporal chaos and intermediate-scale determinism to quantify spatially extended ecosystems. *Proc. Biol. Sci.* 259:111–117.

Biophysical Journal, Volume *110*

Supplemental Information

Emergence of Collagen Orientation Heterogeneity in Healing Infarcts and an Agent-Based Model

William J. Richardson and Jeffrey W. Holmes

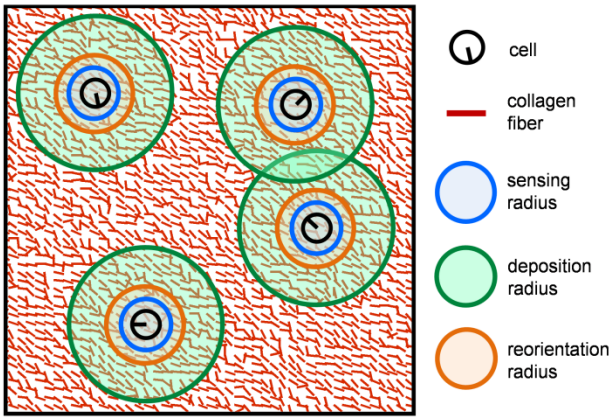

Figure S1: An agent-based model of fibroblast-mediated matrix remodeling.
The model was used to simulate fibroblasts that sense local fiber structure, orient, migrate, deposit collagen, reorient collagen, and degrade collagen. Cell sensing, deposition, and reorientation of collagen occurred over prescribed radii, which were varied in conjunction with varying remodeling rates in order to explore the sensitivity of regional heterogeneity in cell and collagen orientations to those parameters.

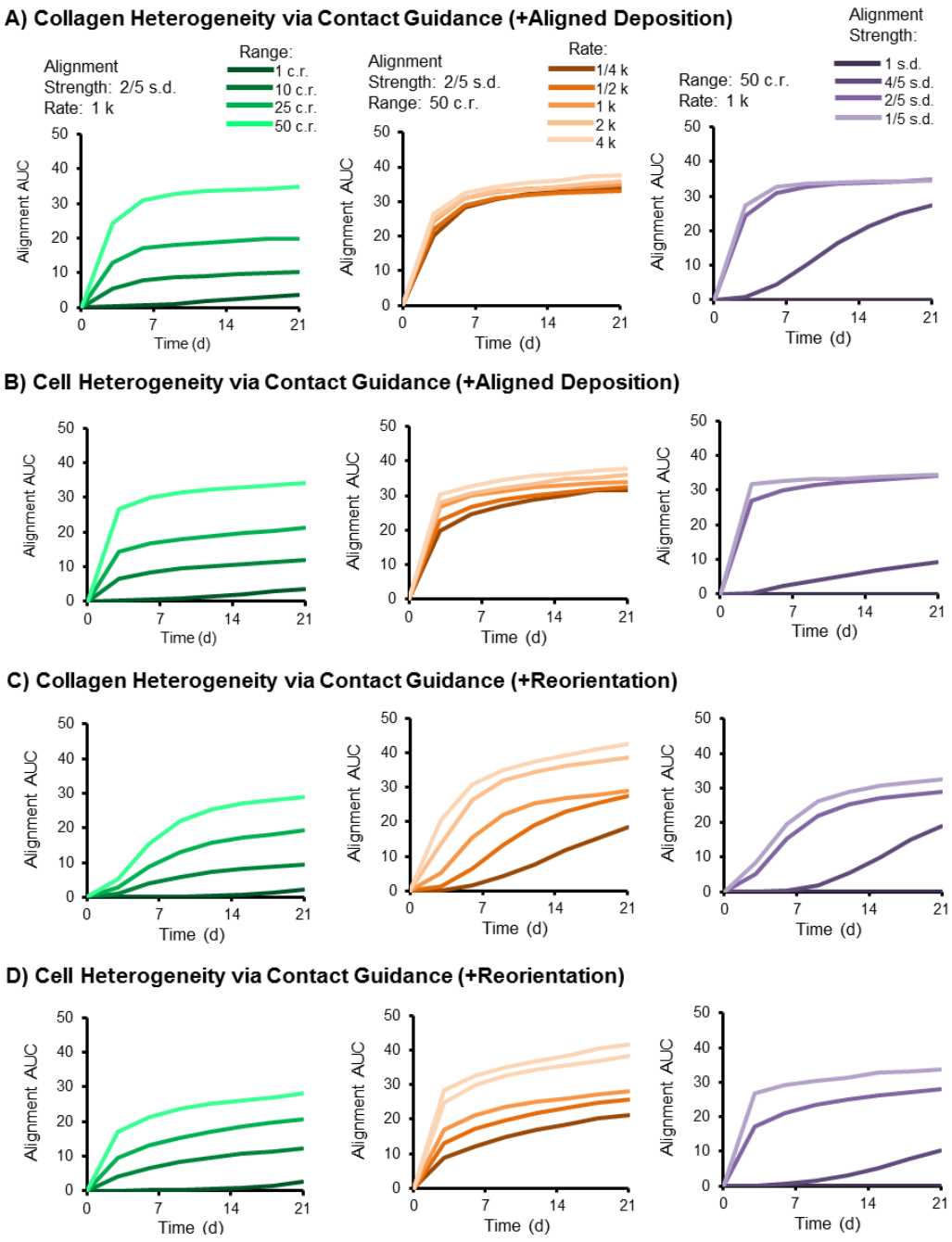

Figure S2: Orientation heterogeneity in long-range sensing simulations.
Cells were set to orient according to collagen fiber orientation distributions sampled across varying distances (i.e., sensing radius), but could only remodel fibers within direct contact (via reorientation or aligned deposition). Heterogeneity in both collagen fiber and cellular orientations (assessed as AUC from alignment vs. distance curves, see Figure 1) increased with the range of sensing (left column), the rate of remodeling (center column), and the strength of the cell alignment probability distribution (right column), but also depended upon the type of remodeling (A-B vs. C-D). Specifically, both long-range sensing with local aligned deposition and long-range sensing with local reorientation produced fiber and cell heterogeneity, aligned deposition generated heterogeneity early and remained steady through 3 weeks while reorientation emerged gradually, aligned deposition was relatively independent of remodeling rate while reorientation was highly dependent on rate, and fiber and cell heterogeneity only emerged at high cell alignment strengths.

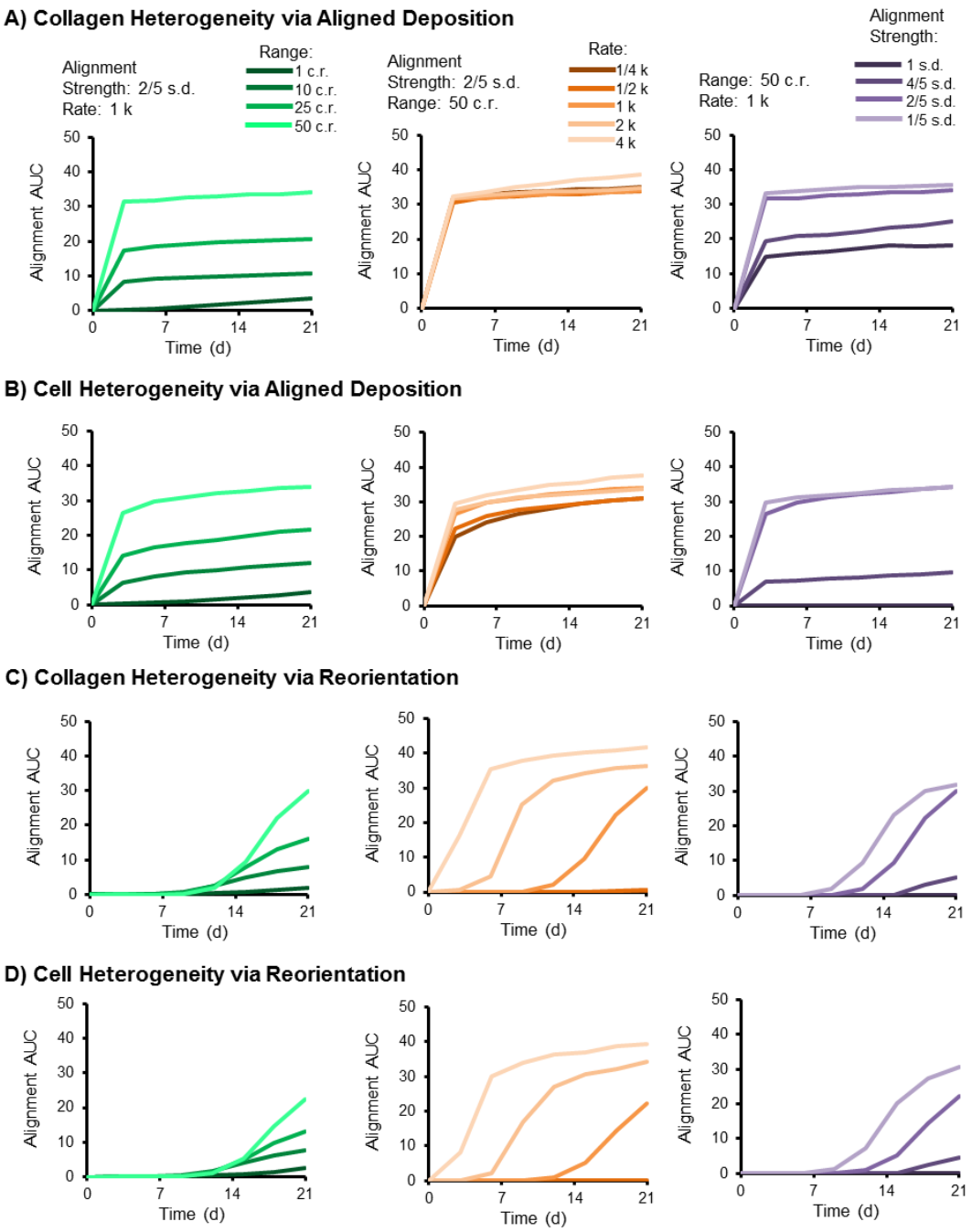

Figure S3: Orientation heterogeneity in long-range remodeling simulations.
Cells were set to remodel fibers across varying distances (i.e., reorientation radius or deposition radius), but could only sense orientation of collagen fibers within direct contact. The degree of regional heterogeneity in collagen fiber & cell orientations (assessed as AUC from alignment vs. distance curves) increased with the range of remodeling (left column), the rate of remodeling (center column), and the strength of the cell alignment probability distribution (right column), but also depended upon the type of remodeling (A-B vs. C-D). Specifically, both long-range aligned deposition and long-range reorientation produced fiber and cell heterogeneity, aligned deposition generated heterogeneity early and remained steady through 3 weeks while reorientation emerged gradually, aligned deposition was relatively independent of remodeling rate while reorientation was highly dependent on rate, and cell heterogeneity only emerged at high cell alignment strengths.